Iranian Journal of Geophysics, Vol 20 No 6, 2027, Page 167 – 188 (Research Article)
DOI: 10.30499/ijg.2025.538402.1720

Soil–pipe interaction and p–y response of buried pipelines under normal faulting: a numerical study

Ali Reza Bagherieh[1*] and Seyed Mohammad Mahdi Mirazim[2]

[1] *Assistant Professor, Department of Civil Engineering, School of Civil Engineering and Architecture, Malayer University, Malayer, Iran*
[2] *M.Sc. in Structural Engineering, Department of Civil Engineering, School of Civil Engineering and Architecture, Malayer University, Malayer, Iran*

(Received: 10 August 2025, Accepted: 02 November 2025)

Abstract

Buried pipelines are vital components of lifeline infrastructure, ensuring the safe and efficient transport of water, gas, and other essential resources. Earthquake-induced fault displacements, however, pose a significant threat to their structural integrity. Numerous numerical studies investigate soil–pipe interaction under fault movement. These approaches, while effective, often require high computational effort, such as modeling the pipeline with shell elements and representing the surrounding soil as a continuum. In practice, engineering analyses frequently adopt Winkler-type spring models to simulate the soil medium, but concerns remain regarding the suitability of this simplified representation and the assignment of p–y responses. To address these limitations, the present study adopts a moderately demanding yet efficient numerical approach. An HDPE pipe buried in sandy soil is subjected to normal faulting at a dip angle of 90°. The pipeline is modeled as a beam element embedded within continuum soil zones with interfacial contact, providing a balance between computational efficiency and modeling accuracy. Comparisons between numerical results and centrifuge test data demonstrate satisfactory agreement. The computed axial and bending strain distributions along the pipeline, as well as the p–y response, align well with centrifuge observations, whereas the ASCE (1984) guideline significantly overestimates the ultimate force and stiffness of the springs. Furthermore, parametric analyses varying design parameters such as burial depth, pipe diameter, and wall thickness show that the numerical trends are physically consistent and provide practical guidance for engineers in selecting optimal values.

.

Keywords: Buried pipelines, FLAC3D, earthquake, faulting, high-density polyethylene

[*]Corresponding author: bagheri@malayeru.ac.ir

1 Introduction

Buried pipelines are an essential part of underground infrastructure in both urban and remote areas. This is especially true for water, gas, and liquid fuel pipelines in remote regions, where burial helps protect them from environmental conditions and human activities. These pipelines are often called lifeline systems because they play a crucial role in ensuring public safety and maintaining the reliability of infrastructure.

It is well established that earthquake-induced permanent ground displacement (PGD) including surface faulting and liquefaction-induced soil movement can significantly affect underground lifelines such as gas and water pipelines. Major damage to these lifelines during earthquakes is often attributed to PGD (Hamada & O'Rourke, 1992; O'Rourke & Liu, 1999).

Several major earthquakes have highlighted the vulnerability of buried lifelines to ground deformation. The 1999 Chi-Chi earthquake in Taiwan caused severe damage to lifeline systems due to fault displacements along the Chelungpu Fault (Tang, 2000). Similarly, the 1999 Kocaeli earthquake in Turkey resulted in extensive damage to the water supply network in Adapazarı, primarily due to ground deformation associated with soil liquefaction and the softening of alluvial sediments (Kurtuluş, 2011). The 2014 Northern Nagano Prefecture earthquake in Japan caused damage to various types of water pipelines, including ductile iron, polyethylene, steel, and PVC pipes, mainly as a result of ground compression near fault zones (Hayashi et al., 2016).
The main types of PGD include faulting induced displacement, landslides, seismic settlement, and lateral spreading due to soil liquefaction. An active fault represents a rupture between two sections of the Earth's crust, along which relative displacement may occur. Whether faulting-induced displacement induces tensile or compressive strains in a pipeline depends on the relative orientation of the pipeline and the fault (e.g., right-lateral or left-lateral displacement). In most cases, both axial and bending strains occur simultaneously during faulting. These strains can lead to rupture as a result of excessive stress or buckling deformation. Such failures not only disrupt the operation of lifeline systems but may also cause serious environmental hazards due to the leakage of dangerous materials, including natural gas, fuel, or liquid waste (Ha et al., 2010).

Given the critical importance of underground lifelines, assessing the seismic response of buried pipelines at fault crossings is a key consideration in seismic design. Ensuring the safety and integrity of pipelines exposed to fault rupture requires particular attention. Consequently, experimental investigations, along with the development of analytical and numerical models capable of accurately predicting pipeline behaviour, are essential. To this end, several two-dimensional physical models have been developed to study the horizontal and vertical resistance of buried pipelines and their associated failure mechanisms. (e.g., Trautmann & O'Rourke, 1985; Ng & Springman, 1994; White et al., 1994; Chin et al., 2006; Cheuk et al., 2008). Fault rupture is inherently a three-dimensional phenomenon and cannot be adequately represented by two-dimensional plane-strain or plane-stress assumptions. The mechanical response of buried pipelines to fault-induced ground displacement is

three-dimensional, and 2D models do not accurately capture in-situ conditions during faulting. Consequently, applying *p–y* curves derived from 2D models to 3D scenarios is generally questionable.

Extensive research has improved understanding of buried pipeline behaviour under fault displacements. Several studies have refined analytical models to more accurately represent bending stiffness and soil–pipe interaction effects (e.g., Takada et al., 2001; Karamitros et al., 2007; Trifonov & Cherniy, 2010, 2012). Numerical modelling approaches have also become increasingly sophisticated, incorporating nonlinear soil springs and shell elements to capture large deformations and plastic behaviour (Shakib & Zia-Tohidi, 2004; Liu et al., 2004; Savidis et al., 2011; Xie, 2008). Parametric investigations have highlighted the influence of soil type, pipeline geometry, and fault–pipeline orientation on mechanical response (Vazouras et al., 2010, 2012, 2015; Tahghighi & Hajnorouzi, 2014; Liu et al., 2016). In addition, recent studies have explored mitigation strategies, such as flexible joints, to enhance pipeline resilience under seismic faulting (Melissianos et al., 2016; Naghdali et al., 2020). Collectively, these advances demonstrate the importance of combining experimental and numerical approaches to accurately predict and improve buried pipeline performance under complex fault-induced ground deformations.

To develop three-dimensional models, Miyajima et al. (2003) and Katagiri et al. (2003) conducted experimental studies on PVC and polyethylene (PE) pipelines subjected to fault rupture. Tohda et al. (2005) performed 3D centrifuge model tests on pipelines under ground settlement. Similarly, Lee (2005) investigated the deformation response of various buried pipelines under reverse faulting using centrifuge modelling, analysing soil reaction forces around the deforming pipe to develop improved analytical approaches for reverse-fault crossings.

Although several physical experiments have been performed to examine 3D soil–pipe interaction, direct measurements of the p–y response of soil under normal faulting remain scarce. Moreover, due to the limited availability of experimental data and the lack of comprehensive validation datasets, further development and calibration of numerical models for such systems are required to ensure their reliability.

Pipelines subjected to faulting-induced displacements generally experience four types of mechanical behavior: pure tension, pure compression, tension with bending, and compression with bending. Typically, pure tension can be viewed as a specific case of tension with bending, and pure compression as a special case of compression with bending. This paper focuses on developing and validating numerical models based on centrifuge experiments simulating tension and bending conditions.

Figure 1 illustrates the general forms of ground rupture that can affect buried pipelines. It shows a pipeline crossing a normal fault at an angle β_n relative to the fault plane, where the pipe experiences both tensile and bending strains. The seismic response of pipelines under normal faulting is typically asymmetric with respect to the fault plane (Xie et al., 2011). The present study specifically focuses on the behaviour of pipelines under normal faulting conditions, i.e., where axial tension occurs in combination with bending strains.

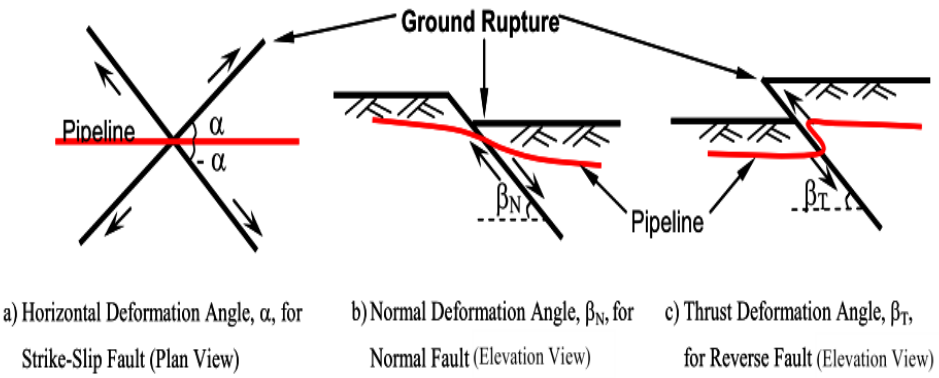

Figure 1. Earthquake-induced ground rupture types: (a) strike-slip, (b) normal, (c) reverse fault (Xie et al., 2011).

Over the past three decades, relatively limited attention has been given to developing analytical models for predicting pipeline behavior under normal or reverse faulting. For pipelines subjected to normal faulting or ground settlement, the distributed soil–pipe interaction forces during downward movement are significantly higher than during upward movement. Kennedy et al. (1977) proposed an analytical method to estimate pipeline strains, though its accuracy is questionable. Nyman (1983) and Murry (1997) developed analytical models for pipelines crossing thaw-unstable zones, conditions that are similar to ground rupture from normal faulting. Ha et al. (2008) used centrifuge modeling to simulate the response of high-density polyethylene (HDPE) pipelines to normal faulting.

Knowledge of the p–y response of soils surrounding buried pipelines, particularly under normal faulting conditions, remains limited. This study aims to address this gap by developing and validating a numerical model for buried HDPE pipelines subjected to normal faulting. The proposed numerical approach embeds beam elements within continuum solid zones, offering a reasonable balance between computational efficiency and modeling accuracy. It is neither as simplistic as the Winkler spring model nor as computationally demanding as shell-element modeling within a continuum. The primary objective of this study is to verify whether the p–y response predicted by the proposed approach is consistent with the results obtained from centrifuge experiments. The findings provide a foundation for more reliable design and assessment of lifeline systems crossing active faults.

2 Centrifuge Modeling of HDPE Pipe under Normal Fault

The centrifuge test involves simulating geotechnical phenomena using small-scale models subjected to self-weight stresses equivalent to several times Earth's gravity. Centrifuge model testing has proven particularly valuable for elucidating deformation and failure mechanisms and for providing data to validate numerical analyses (Taylor, 1995). The fundamental principle of centrifuge modeling is the 1/N scale model tested under a gravitational field of Ng, where N is the scale factor and g is the gravitational acceleration (Table 1).

Table 1. Centrifuge Scaling Laws.

Parameter	Unit	Scale
Acceleration	L/T^2	n
Linear dimension	L	1/n
Area dimension	L^2	$1/n^2$
Volume dimension	L^3	$1/n^3$
Stress	M/LT^2	1
Strain	-	1
Mass	M	$1/n^3$
Density	M/L^3	1
Unit weight	$M/(L^2T^2)$	n
Force	ML/T^2	$1/n^2$
Bending Moment	ML^2/T^2	$1/n^3$

In the centrifuge tests conducted by Ha et al. (2008), fault displacements were simulated using a split-box container with internal dimensions of 1.14 m × 0.76 m × 0.2 m (Figure 2). This container was capable of reproducing both vertical and horizontal displacements while the centrifuge was in operation. The maximum vertical displacement that could be applied by the split box was approximately 0.04 m, corresponding to an equivalent prototype displacement of 0.48 m at a scale factor of 12.2g.

The modelled pipe was hinged to the walls of the split box, simulating the prototype pipe with compression blocks near the fault. Axial and bending strains in the pipe were recorded during the simulated fault displacement, while lateral forces along the pipeline were measured using tactile pressure sensors. The observed lateral force distributions were consistent with the values inferred from strain gauge measurements. In the normal fault scenario, lateral forces on the pipe were asymmetric relative to the fault, with a concentration on the uplift side. The maximum lateral force was compared with the data provided in the ASCE (1984) guideline and experimental results used to develop the full p–y soil–pipe interaction relationship. For a normal fault, the ASCE (1984) guideline proposes a p–y curve characterised by a high maximum bearing capacity and a steep slope (i.e., small yield displacement), which was adopted in the present study as a reference for evaluating both the experimental tests and 3D numerical modelling results.

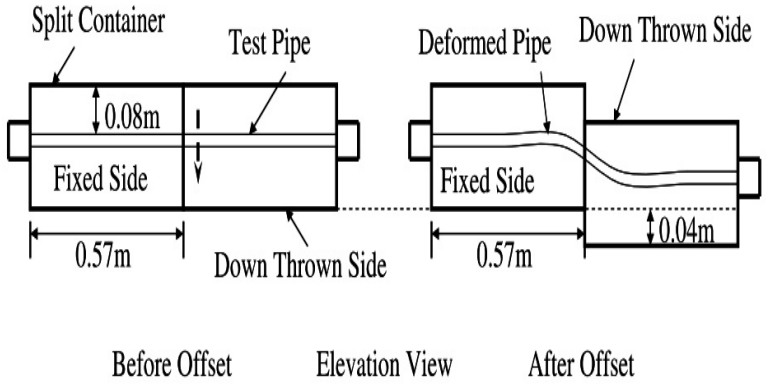

Figure 2. Centrifuge Model Setup Before and After Displacement in Normal Fault Simulation, Elevation View (Ha, 2007).

3 Three-Dimensional Numerical Modeling of Buried Pipelines

3.1 Numerical Modelling Software

FLAC3D is a numerical modelling program for continuum media that can effectively simulate the behaviour of soil and rock under structural loads. It

employs an explicit finite difference method based on Lagrangian calculations, enabling accurate computation of point displacements under large-strain conditions (Itasca Consulting Group, 2020). Consequently, Lagrangian-based analysis is particularly suitable for PGD problems involving large strains. While implicit solutions for complex continuum analyses can be very time-consuming, FLAC's explicit approach provides accurate model responses within a relatively short computation time. Because FLAC does not generate a stiffness matrix, it also requires relatively low computer memory. The program is capable of simulating both elastic and plastic material behaviour.

3.2 Geometric Characteristics of the Model and HDPE Pipe Specifications

In this study, the pipeline was assumed to be straight, with uniform surrounding soil. Soil properties, burial depth, and pipe cross-section characteristics were considered constant along the pipeline. The effects of pipeline joints were neglected; in other words, the pipeline was assumed to be continuous.

The geometric specifications, model properties, and boundary conditions for the pipeline model generated in FLAC were adopted from the centrifuge model. The model dimensions in the X, Y, and Z coordinate directions were 1.14 m, 0.76 m, and 0.2 m, respectively, matching the internal dimensions of the split-box container used in the centrifuge device (Figure 3).

In FLAC3D, the meshing process is entirely user-controlled and is not automatically generated. The user defines the initial dimensions of the blocks (zones) when creating the model, specifying the number of zones along each direction. Once the initial mesh is established, the user can manually refine it or adjust certain features of the zone geometry to improve resolution in critical regions.

In this study, the zone size was selected to achieve an optimal balance between numerical accuracy and computational efficiency. Larger zones may introduce numerical errors, while excessively small zones substantially increase computation time. This issue is particularly critical because FLAC3D employs an explicit solution scheme, which generally requires smaller time steps and therefore greater computational effort compared to conventional implicit finite element methods. The optimal zone size was determined through a trial-and-error procedure by varying the mesh density until a reasonable agreement was achieved between the numerical and experimental results, and further mesh refinement did not produce significant changes in the overall response trends. In the present study, a mesh of $20 \times 10 \times 5$ zones (a total of 1,000 zones) was utilized for modeling.

The soil was modeled using the Mohr–Coulomb constitutive model, which includes the material parameters of shear modulus (G), Poisson's ratio (ν), friction angle (φ), and cohesion (c). The values of these parameters are presented in Table 2, as reported by Ha et al. (2008) and Xie (2008). Although the traditional Mohr–Coulomb model has certain limitations, particularly its inability to accurately represent strain-softening behavior, several modified versions have been proposed to address these shortcomings (e.g., Robert & Rajeev, 2016; Chatzidakis et al., 2022). Nevertheless, the original form of the model remains widely adopted for this

type of analysis (e.g., Farhang & Hojat Jalai, 2025; Dimirci et al., 2018; Banushi et al., 2018). Since the primary objective of this study is to obtain realistic predictions of faulting-induced strains and soil–structure interaction forces using a numerical scheme with relatively low computational demand, the selected constitutive model is considered sufficient to represent the soil failure mechanism and its ultimate resistance (bearing capacity).

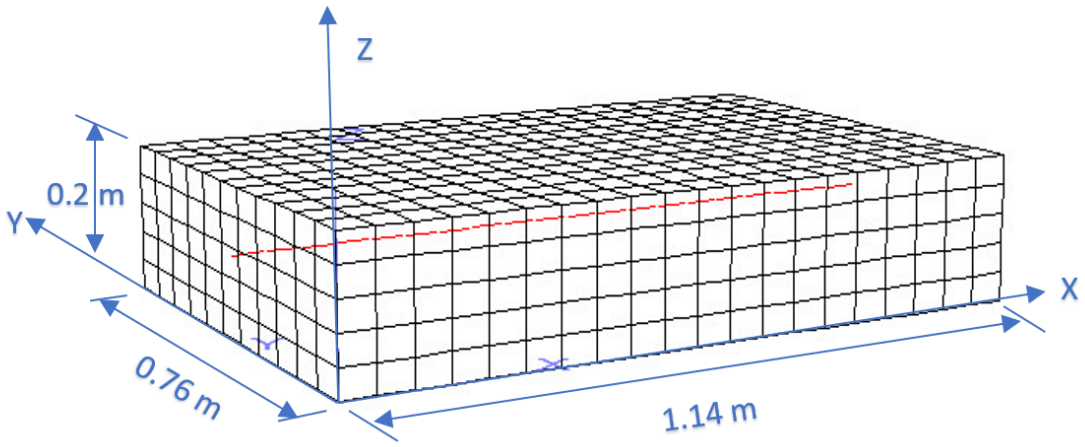

Figure 3. Geometry and mesh of the modeled soil with the embedded pipeline in FLAC3D.

When modeling buried pipelines subjected to fault-induced displacements, the use of beam elements is a well-established and practical approach. This method can effectively capture the elasto-plastic behavior and frictional properties of the surrounding soil (Joshi et al., 2011; Xie et al., 2011). Such models are relatively straightforward to construct and analyze, making them suitable for practical engineering applications (Talebi & Kiyono, 2021). They can also be executed on personal computers within reasonable computation times, which is advantageous for iterative design processes. Moreover, beam–spring models are capable of simulating the formation of plastic hinges and capturing both tensile and compressive strains along the pipeline (Uckan et al., 2015).

In the present study, numerical simulations of the HDPE pipe under a normal fault with a fault plane dip angle $\beta = 90°$ were performed in FLAC3D using pile elements which is a specialized form of structural beam element. It is a two-node (line) structural member whose nodes coincide with FLAC3D grid points. The element itself is one-dimensional and has no physical volume; its interaction with the surrounding continuum occurs through its nodes. Compared to conventional beam elements, pile elements are specifically designed to simulate distributed axial and shear force transfer between the soil and the structural member. They are therefore well suited for soil–structure interaction problems involving buried piles, pipes, or shafts. The pile element includes built-in distributed coupling springs (normal and shear) along its length, which automatically represent soil reactions through link elements.

The reduced friction angle between the pipe and the surrounding soil was

taken as two-thirds of the soil's internal friction angle φ (Yimsiri et al., 2004). For dense sand (φ = 40°), this corresponds to a pipe–soil friction coefficient μ = 0.5 (Xie, 2008).

The modeled pipe in FLAC3D had a length of 1.14 m, an outer diameter D of 33.4 mm, a wall thickness t of 1.96 mm, and a burial depth to the pipe center H_c of 0.092 m (H_c/D = 2.8), matching the centrifuge scale.

Table 2. Soil parameters used in the numerical analysis (Ha, 2007).

Parameter	Dense Sand Value
Shear modulus *G* (MPa)	9.5
Unit weight γ (kN/m³)	14.7
Poisson's ratio ν	0.3
Internal friction angle φ (°)	40
Dilation angle ψ (°)	0
Cohesion *c* (kPa)	0
Pipe–soil friction coefficient μ	0.5

All centrifuge tests were conducted with relatively low fault displacement rates, resulting in low strain rates in the pipe material. However, some tests were performed at higher displacement rates to examine their influence on pipeline response. It should be noted that, due to the static nature of the FLAC model, the effect of fault displacement rate was neglected in the analysis, and the simulations were controlled by the final displacement value.

The stress–strain relationship for HDPE pipe material is nonlinear and strain-rate dependent. A hyperbolic empirical model proposed by Merry and Berry (1997), which incorporates strain-rate effects, was used for modeling purposes. Although this model shows good agreement with laboratory data at a strain rate of 1%/min, significant deviations occur at higher strain rates, limiting its applicability (Figure 5). In this study, consistent with the centrifuge tests, a strain rate of 1%/min was adopted.

For simplification, the pipe material was assumed to be elastic, and its stress–strain relationship was considered linear. Thus, Young's modulus and the tensile (compressive) yield strength of the pipe material were taken as 400 MPa and 13.6 MPa, respectively, based on Figure 4 and the selected strain rate. In accordance with centrifuge test data, due to the high compaction of the HDPE material, a density of 955 kg/m³ and a Poisson's ratio of 0.45 were used for the pipe in the model.

The pipe was loaded in two stages: first, a geostatic analysis was performed to establish the initial stress state in the soil; second, a vertical displacement (normal fault simulation) was applied to all nodes that were free to move vertically. As the normal fault movement progressed, the soil in the fault zone underwent very large deformations.

As noted, the faulting process can be considered a static problem; the speed and rate of fault displacement have little effect on the stresses and strains induced in pipelines. Instead, the final displacement magnitude is of primary importance. Therefore, in the fault modeling, one side of the fault was fixed, while all points on the other side of the fault (from X = 0.75 m to X = 1.14 m) were assigned a specified vertical velocity in the negative Z-direction. Due to the restraining effect of the soil, the relative displacement between the soil and the pipe at the fault location induced both axial and lateral forces on the pipeline.

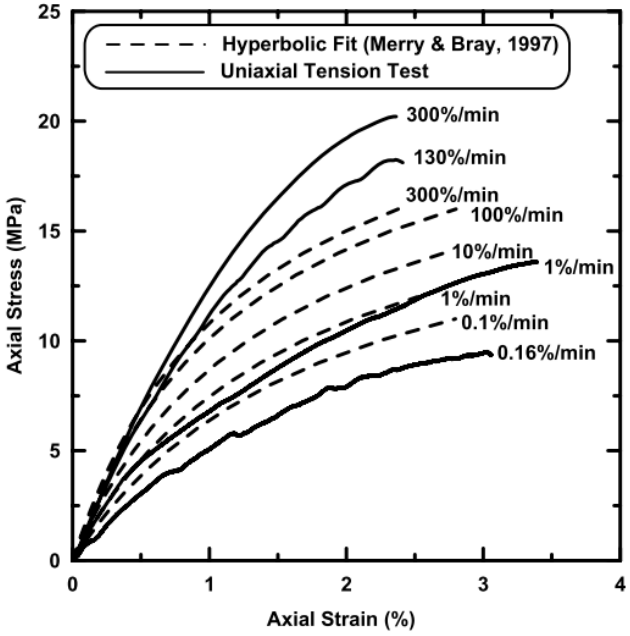

Figure 4. Stress–strain relationship of dense HDPE at different strain rates (adapted from Ha, 2010).

In this study, a normal fault with continuous soil–pipe contact was modeled to closely match real conditions. In previous studies, the soil around the pipe was represented using nonlinear elasto-plastic springs in axial, lateral, and vertical directions, generating a specified resistance per unit pipe length without considering actual contact effects. Soil resistance depends on soil properties and applied stresses, and is therefore not uniform along the pipe. In contrast, in Winkler spring–based simulations (Winkler, 1867), the same elasto-plastic spring properties are applied to all surrounding soil. The continuous model used here avoids such simplifications and allows each point to respond according to its geometric location and stress state.

3.3 Pipe–Soil p–y Response under PGD

In analytical and many computational models for studying soil–pipeline interaction, force–displacement relationships, which represent the movement of soil relative to the pipeline, are essential. The nonlinear stress-dependent characteristics of these force–deformation curves are expressed by springs, commonly represented as *t–x*, *p–y*, and *q–z* curves (Figure 5), which describe the soil behavior in axial, lateral horizontal, and lateral vertical directions, respectively. Some of the widely used lateral force–displacement relationships, often referred to as *p–y* curves, were provided by the ASCE Gas and Liquid Fuel Lifelines Committee in its seismic design guidelines for oil and gas pipeline systems (ASCE, 1984). It should be noted that, for normal faulting, the axial and horizontal lateral directions are not of primary importance. The ASCE (1984) guidelines provide a bilinear relationship for the transverse force of pipeline–soil interaction.

The elasto-plastic relationship is determined by the maximum force per unit length corresponding to the section of the pipeline that bears the downward

soil load during fault displacement (ASCE, 1984):

$$q_{ud} = N_{qd}\gamma H_c + \frac{1}{2}\gamma N_r D^2 \quad (1)$$

and its relative displacement,

$$Z_{ud} = (0.1 \rightarrow 0.15)D \quad (2)$$

In these equations, N_{qd} and N_r are dimensionless factors for the vertical downward load of a horizontal strip footing in dense sand. For the centrifuge experiments described above, with prototype scale parameters: γ=14.37 kN/m^3, Hc=1.12m, D=0.408m where γ is the effective unit weight density of the soil, Hc is the depth of the soil from the ground surface to the center of the pipe, and D is the pipe. N_{qd} and N_r from the ASCE guidelines are calculated 65 and 80 respectively, the results are: q_{ud}=536 kN/m and Z_{ud}≈0.05 m.

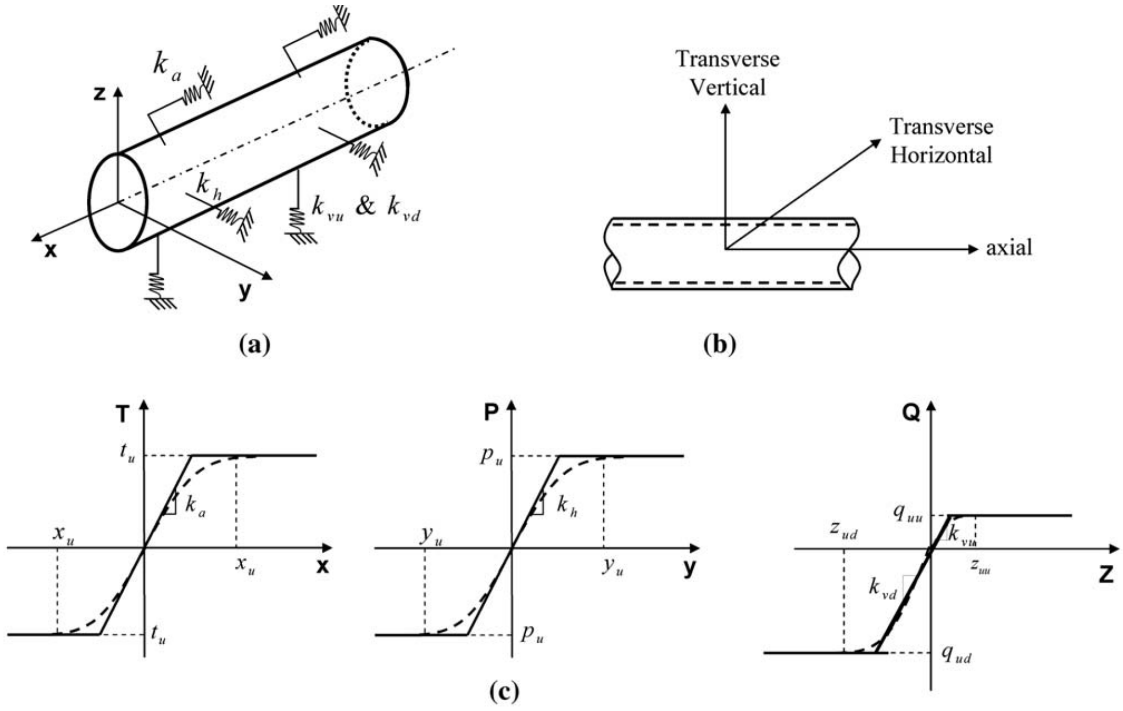

Figure 5. Winkler spring model as defined in ASCE (1984) guidelines.

The three-dimensional behavior and interaction between soil and pipe under normal faulting is a complex phenomenon. A series of numerical models based on the finite difference method were developed to study the soil–pipe interaction in three dimensions (using pile elements for the pipe and a continuum model for the soil).

The objectives of the finite difference analysis in this study are, more specifically, to examine the applicability of continuum modeling as an alternative to spring models by comparing results with centrifuge experiments, and to calibrate the soil–pipe interaction (*p*–*y*) relationship for normal faulting conditions based on centrifuge test data.

The priorities of this research are first to investigate the soil pressure acting on the pipe, and then the pipe deformation and strain due to changes in soil pressure. In the three-dimensional continuum analysis, the soil–pipe interaction in the section of the pipeline near the fault (at a distance of 1.5D from

the fault trace where the strongest influence on the pipeline response occurs, was examined. Specifically, as the distance from the fault increases, the maximum displacement generally decreases. The computed pipe resistance curve (*p–y*) was generated and compared with the *p–y* relationships defined in the ASCE (1984) guidelines. The forces obtained as a function of normalized pipe displacement (y/D) are shown in Figure 6.

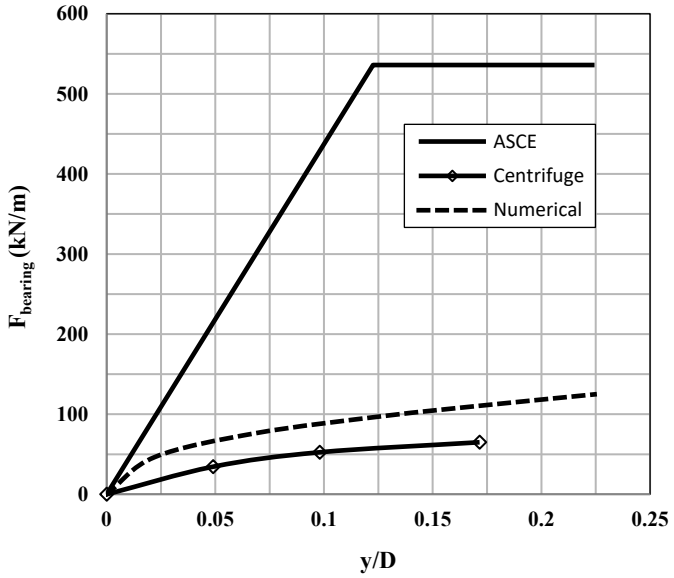

Figure 6. Bearing capacity from ASCE (1984) guidelines, centrifuge.

experiments (Ha, 2008), and numerical modeling results of the present study

The numerical simulation results shown in Figure 6 exhibit acceptable agreement with the experimental results. The small discrepancies between the numerical and experimental results may be partly attributed to the fact that, in the centrifuge tests with a gravity scale of 12.2g, the real confinement conditions for dense sand could not be fully replicated due to sensor attachment on the pipe surface. Although the numerical model's bearing capacity curve differs considerably from that given by the ASCE (1984) guidelines, it maintains an elasto-plastic form consistent with physical reality.

Due to equipment limitations and the displacement range that could be imposed for normal faulting, the maximum bearing resistance did not reach a plateau in the curve. The significant differences in the curves shown in Figure 7 indicate that designing HDPE pipelines for normal faulting solely based on the ASCE (1984) guidelines may be considered conservative.

4 Numerical Analysis of Buried Pipeline under Normal Faulting

The examination of predicted strain distributions indicates that these simulations significantly overestimate the measured axial and bending strains (for example, the ASCE guideline is overly conservative). The axial and bending strains from the numerical simulation of normal faulting and the centrifuge test results (Ha, 2008) are shown in Figure 7. The modeling was

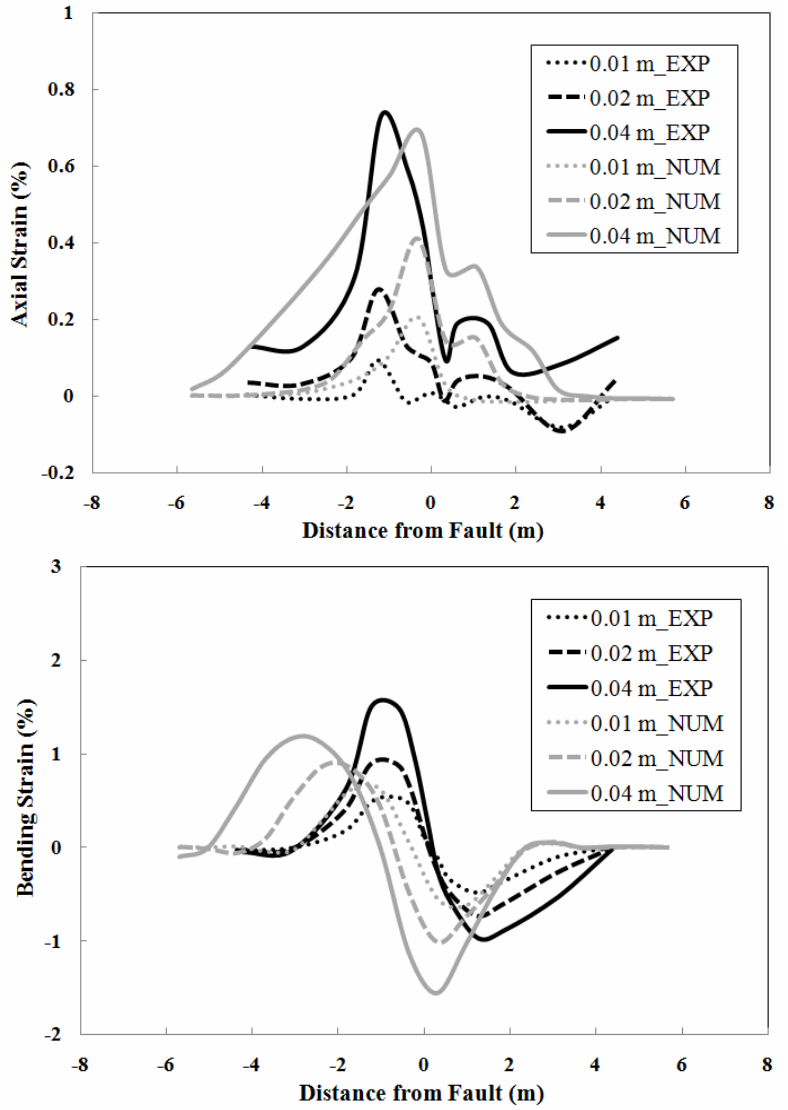

Figure 7. Distribution of measured and predicted axial and bending strains along the pipeline.

performed for three different fault displacements of 0.04, 0.02, and 0.01 meters (equivalent to 0.488, 0.244, and 0.122 meters in prototype scale) consistent with the centrifuge test data.

In this study, the axial strain is considered to be caused solely by direct tension or compression, while bending strain arises only from transverse bending. As observed in Figure 7, there is good agreement between numerical and experimental results; both the numerical predictions and centrifuge data show that for normal faulting at a 90° angle, a large vertical force is concentrated near the fault in the fixed, non-moving region of the model. This large vertical force arises from asymmetry in soil resistance, which is high in the fixed region and low in the part of the model displaced downward. The numerical results indicate that as fault displacement increases, the asymmetry in soil resistance causes a displacement and transfer at the opposite side of bending. Interestingly, this

displacement transfer was not observed in the experimental data. As noted, variations in soil resistance in the vertical direction and in the region to the right of the fault affect bending strain more than axial strain. The predicted axial strain reaches its maximum at approximately 2 meters on both sides of the fault location.

Part of the discrepancy between the numerical and experimental axial strain values shown in Figure 8 is due to approximations in the numerical solution of the equations. Additionally, there are limitations in using the Mohr-Coulomb failure criterion to simulate soil flow. Another explanation for these differences lies in the limitations of the centrifuge tests due to the presence of sensors. The first limitation relates to strain gauges and errors caused by local hardening effects in model pipes with low stiffness. To appropriately model the geometry and bending stiffness of a wide range of pipeline materials (e.g., steel, cast iron, high-density polyethylene (HDPE)), strain is measured on aluminum model pipes representing materials with low plastic stiffness. For materials with low stiffness, the local bending stiffness of the model pipe increases due to the application of adhesive strain gauges and the stiffness of the strain gauges themselves. Research in geosynthetics has shown that this local hardening effect results in significant strain measurement errors (e.g., Bathurst et al., 2002; Warren et al., 2010). Therefore, this strain measurement technique is not suitable for physical modeling of flexible pipeline materials. The second limitation of strain gauge technology is that strain gauges provide point measurements of strain. Thus, to obtain the maximum curvature along a pipeline exposed to bending under differential ground displacement, many strain gauges are required. However, the number of instruments that can be used is limited by practical constraints such as minimum spacing between sensors, wiring, and other related installation systems. Another factor to consider is that the soil surrounding the pipe may not be properly compacted due to the presence of these sensors.

It is important to note that the bending strain at the fault location should be negligible and close to zero. It should also be mentioned that the mesh size in the fault zone of the numerical model influences the variation of bending strain distribution along the pipeline length; the smaller the mesh size at the fault location, the smaller the differences in results, and the closer the model approximates reality. Nonetheless, an overall satisfactory comparison between experimental data and numerical simulation indicates that finite difference models reasonably capture the soil–pipe interaction and overall strain response. It should be noted that due to equipment limitations, the normal fault displacement in the prototype sample cannot exceed 0.48 meters.

The peak axial and bending strains from the numerical analyses and centrifuge test results are plotted against fault displacement in Figure 8. As observed, the peak axial strain versus fault displacement is similar in both modeling approaches. In this figure, a slight deviation from linear behavior (partial hardening) in centrifuge test results appears at displacements greater than 0.3 meters. The maximum bending strains on both sides of the fault location differ, and here too, a slight deviation (partial softening) from linear behavior is observed.

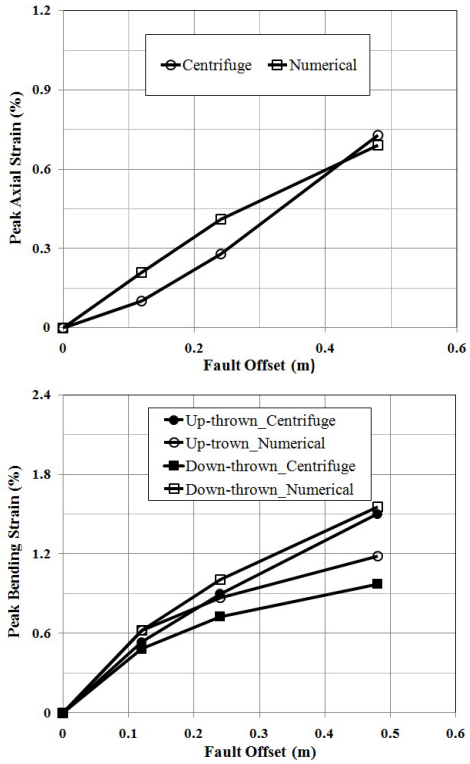

Figure 8. Maximum axial and bending strains versus normal fault displacement at β = 90°.

5 Parametric Analysis of Buried Pipeline under Normal Faulting

This section presents a parametric study on factors affecting the distribution of axial and bending strains along the pipeline, including burial depth, pipe diameter, pipe wall thickness, and pipe material stiffness. In all cases, the obtained strain distribution curves are compared with the numerical modeling results of normal faulting. It is worth noting that all pipeline simulations employed polyethylene pipes conforming to the AWWA standard.

The primary objective of numerical parametric analyses is, first, to evaluate the influence of various parameters on the behavior of buried pipelines. The results provide practical engineers with valuable insights into how each parameter affects pipeline response and aid in identifying optimal combinations of design parameters. By understanding the trends associated with each parameter, optimizing pipe wall thickness, burial depth, and soil conditions becomes critical for enhancing pipeline resilience against fault-induced ground movements. Second, comparing the outcomes of this study with those from other published numerical or experimental investigations helps validate the numerical schemes employed.

5.1 Effect of Burial Depth (H/D Ratio)

According to ASCE (1984) guidelines and Yimsiri (2004), the relative burial depth, expressed as the ratio of burial depth to pipe diameter (H_c/D), is the primary parameter influencing lateral soil–pipe interaction. The effect of this parameter was investigated for a nominal H_c/D ratio of approximately 5, using different combinations of pipe diameters and burial depths. In one scenario, the pipe diameter was fixed while burial depth increased (H/D = 5); in the other, burial depth was fixed while pipe diameter decreased (H/D = 5.1) (Figures 9 and 10).

As expected, in the first scenario, increased soil resistance at greater burial depths leads to higher axial and bending strains, particularly at larger fault displacements. Figure 9 shows that as burial depth increases, bending deformation becomes concentrated closer to the fault, with the location of maximum bending strain shifting toward the fault line and its magnitude increasing due to higher soil resistance. Measured axial strains for H/D = 5 are also more concentrated near the fault, reflecting higher longitudinal friction compared to H/D = 2.8, although axial strains remain similar for small fault displacements.

When the burial depth increases, the higher confinement of the surrounding soil caused by overburden pressure forces the pipeline to follow the abrupt fault-induced deformations transferred through the stiffer soil. As a result, the curvature of the beam increases, and the bending strains become more pronounced. At the same time, the frictional resistance between the soil and the pipe surface is enhanced, leading to higher axial strains. This observation agrees with the findings of Qiu et al. (2025), who reported that a lower H/D ratio improves deformation compatibility and enhances the overall structural stability of the pipeline.

5.2 Effect of Pipe Diameter

The effect of pipe diameter was investigated at H/D =5.1, where the pipe diameter is approximately half that of the case with H/D = 2.8. The axial and bending strain distributions along the pipe are presented in Figure 10. Comparison of strain distributions for larger and smaller diameter pipes at the same burial depth indicates that pipe diameter has a relatively minor effect on axial strain distribution. However, bending strains in the smaller diameter pipe model are slightly lower than those in the larger diameter pipe model. This observation is consistent with the findings of Wijewickreme and Dilrukshi (2017), who reported that, for a given overburden ratio or burial depth (H), the normalized maximum soil restraint decreases with increasing pipe diameter (D). A larger soil restraint at smaller diameters indicates a stronger resistance of the surrounding soil against pipe movement, resulting in greater curvature along the pipe and, consequently, higher bending and axial strains.

Although the H/D ratio is a convenient dimensionless parameter that simplifies the interpretation of soil–pipe interaction results, the present study demonstrates that the individual values of burial depth (H) and pipe diameter (D) also exert distinct influences on pipeline response. Therefore, both parameters should be explicitly considered when evaluating soil restraint and the resulting axial and bending strain distributions. In general, factors affecting pipeline behavior are highly interactive. For this reason, Dey and Tesfamariam (2022) employed the Taguchi method and design of experiments to identify the key factors, including pipe diameter-to-wall thickness ratio (D/t), burial depth, soil stiffness, and fault angle, that influence pipeline response.

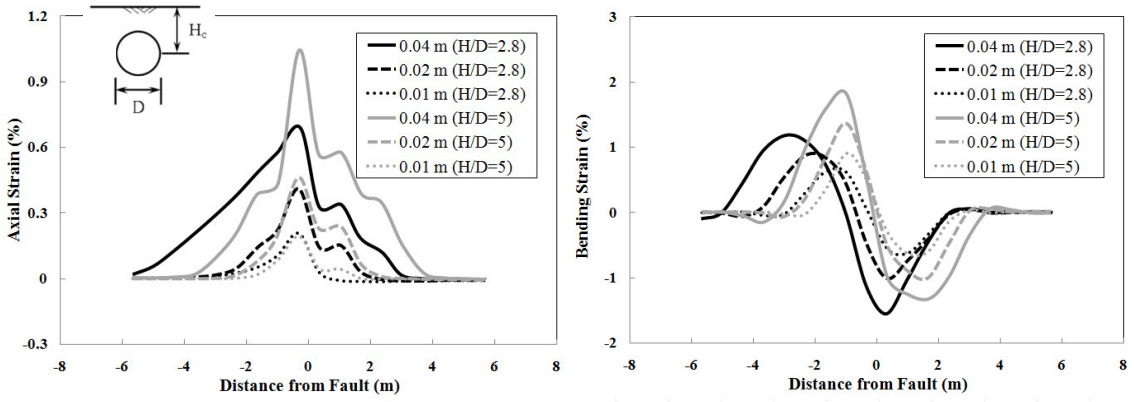

Figure 9. Effect of burial depth on the distribution of axial and bending strains in normal faulting.

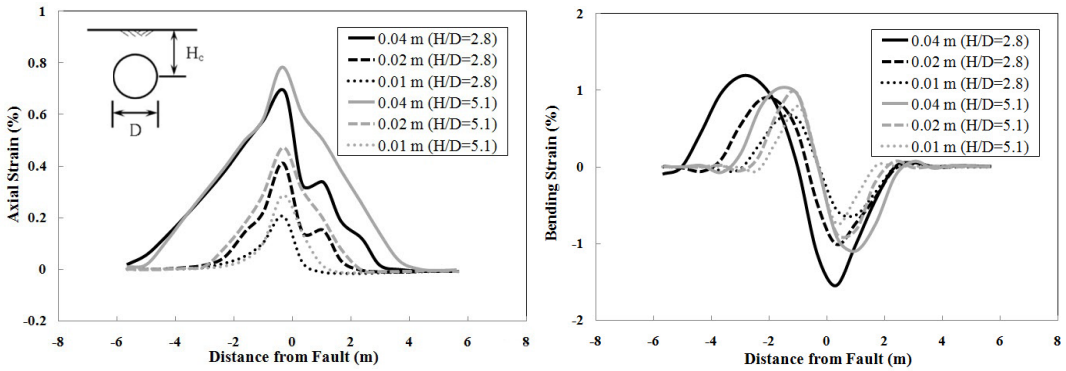

Figure 10. Effect of pipe diameter on the distribution of axial and bending strains in normal faulting.

5.3 Effect of Pipe Wall Thickness (D/t Ratio)

The diameter-to-thickness (D/t) ratio emerging as a key design parameter influencing mechanical performance under faulting hazards. Understanding how D/t ratio affects strain and stress responses is essential for ensuring pipeline safety, seismic resilience, and long-term infrastructure reliability (Jahangiri and Shakib, 2020). The influence of pipe wall thickness on the distribution of axial and bending strains was investigated at a fault displacement of 0.04 m in the centrifuge model (0.448 m in the prototype scale) for different D/t ratios, with a constant pipe diameter of 0.3344 m (centrifuge scale) (Figure 11). Specifically, D/t = 11 (t = 0.0304 m) was selected as the thick-wall case, and D/t = 26 (t = 0.0129 m) as the thin-wall case, in addition to previous results for D/t = 17 (t = 0.0196 m). As shown in Figure 11, increasing the pipe wall thickness leads to reductions in both maximum axial and bending strains. This behavior is attributed to the increased cross-sectional area, moment of inertia, and bending stiffness associated with greater wall thickness. This observation aligns with the findings of Zhang et al. (2020), who reported that pipeline axial strain decreases with a lower diameter-to-thickness ratio (D/t). Therefore, a lower diameter-to-thickness ratio (D/t) generally results in decreased axial strain in pipelines, enhancing their structural integrity and resistance to faulting displacements.

5.4 Effect of Pipe Material Stiffness

This section examines the effect of the pipe material's elastic modulus on the distribution of axial and bending strains.

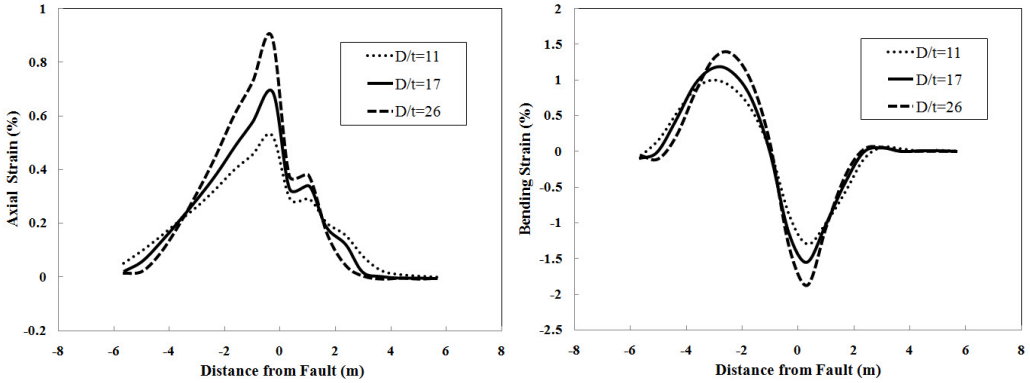

Figure 11. Effect of pipe wall thickness on the distribution of axial and bending strains under a normal fault displacement of 0.488 m in prototype scale.

For simplicity, the pipe materials were assumed to be elastic with linear stress–strain behavior. As shown in Figure 12, the overall shape and pattern of the axial and bending strain distributions remain similar, while increasing the material stiffness reduces both axial and bending strains. The influence of material stiffness on strain distribution is particularly pronounced at larger fault displacements.

The bending strain is directly related to pipe curvature, which is a function of the pipe bending stiffness (E_pI_p). A higher bending stiffness limits the curvature induced by soil–pipe interaction, thereby reducing bending strain, as demonstrated in previous studies (e.g., Saiyar et al. 2016). In addition, a stiffer pipe resists local deformations imposed by the fault displacement, which distributes the displacement over a longer pipe length and reduces the corresponding axial strain. These observations are consistent with the physical behavior of the soil–pipe system and justify the trends observed in the numerical results.

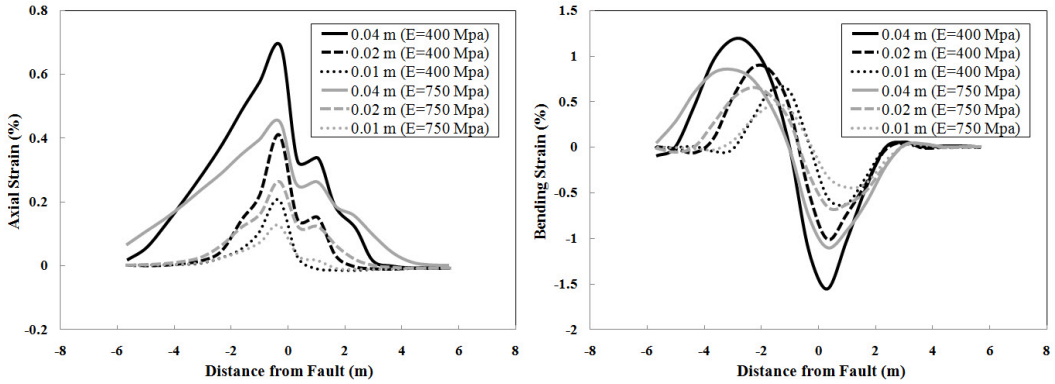

Figure 12. Effect of material stiffness on the distribution of axial and bending strains under normal faulting.

6 Conclusions

This study employed a numerical approach to model the response of buried pipelines subjected to normal fault displacements, where beam elements were embedded within solid elements representing the surrounding soil. The results showed good agreement with measured bending and axial strains, demonstrating that the proposed method can reliably capture the key aspects of soil–pipe interaction under fault movement.

The adopted approach is more realistic than the simplified Winkler spring model, yet far less computationally demanding than continuum models using shell elements, which typically require high-performance computing resources. It therefore offers a balanced compromise between accuracy and efficiency. By directly modelling the interaction between soil and pipe, the method reduces the assumptions and uncertainties associated with selecting appropriate spring stiffness values in conventional analyses.

It should be noted that the present model does not account for local buckling of pipelines, which may occur under very large fault offsets or in thin-walled pipes. However, such situations are generally avoided in practical pipeline design. Hence, the proposed approach can serve as a reliable and practical tool for design applications, especially when iterative or trial-and-error analyses are required to identify

optimal combinations of design parameters such as burial depth, wall thickness, and pipe diameter.

The results also highlight the importance of accurately defining Winkler spring stiffness, as commonly used guidelines may not provide sufficient precision for this type of problem.

Parametric analyses confirmed that the trends obtained are consistent with previous studies. Increasing burial depth leads to higher soil confinement, forcing the pipeline to follow the abrupt fault-induced deformation within the stiffer surrounding soil. This results in increased curvature and higher bending strains. At the same time, greater frictional resistance along the pipe–soil interface causes an increase in axial strain.

At a constant burial depth, pipe diameter has a relatively minor effect on axial strain distribution; however, bending strains in smaller-diameter pipes are slightly lower than those in larger pipes. Although the burial depth ratio $H/D$is a convenient dimensionless parameter for interpreting soil–pipe interaction, this study demonstrates that both burial depth (H) and pipe diameter (D) individually influence pipeline behaviour and should therefore be considered explicitly.

A lower diameter-to-thickness ratio (D/t) was found to reduce axial strain, thereby improving the pipeline's structural integrity and resistance to faulting displacements.

A stiffer pipe material can better resist local deformations imposed by fault movement, distributing the displacement over a longer pipe length and reducing the corresponding strain.

Overall, the observed trends provide valuable insights for design engineers, offering realistic guidance for selecting appropriate design parameters and improving the resilience of buried pipelines against normal faulting. It should be noted, however, that the present results correspond to a normal fault with a dip angle of 90° and a HDPE pipeline embedded in dense sand; different materials, fault geometries, or soil types may lead to varying trends.

Table 7. List of Symbols.

Symbol	Description	Unit
X, Y, Z	Cartesian coordinate directions	m
D	Pipe outer diameter	m
t	Pipe wall thickness	m
H_c	Burial depth to pipe center	m
H_c/D	Dimensionless burial depth ratio	–
G	Shear modulus of soil	MPa
ν	Poisson's ratio	–
ϕ	Internal friction angle of soil	°
ψ	Dilation angle of soil	°
c	Cohesion of soil	kPa
γ	Unit weight (effective weight density) of soil	kN/m³
μ	Pipe–soil friction coefficient	–
E	Young's modulus of pipe material	MPa
ρ	Density of pipe material	kg/m³
q_{ud}	Ultimate downward soil reaction per unit pipe length	kN/m
Z_{ud}	Relative displacement corresponding to q_{ud}	m

Symbol	Description	Unit
N_{qd}, N_r	Dimensionless bearing capacity factors	–
p	Lateral soil resistance per unit length (p–y response)	kN/m
y	Lateral pipe displacement	m
t–x	Axial force–displacement response	–
q–z	Vertical force–displacement response	–
D/t	Diameter-to-thickness ratio	–
σ_y	Yield strength of pipe material (tensile/compressive)	MPa
ε	Strain	–
β	Fault dip angle	°
δ	Pipe–soil interface friction angle	°

References

American Water Works Association. (2003). AWWA Standard for Polyethylene (PE) Pressure Pipe and Tubing, 1/2 in. (13 mm) Through 3 in. (76 mm), for Water Service (ANSI/AWWA C901-02).

ASCE. (1984). Guidelines for the Seismic Design of Oil and Gas Pipeline Systems. Committee on Gas and Liquid Fuel Lifelines, American Society of Civil Engineers, Reston, VA.

Banushi, G., Squeglia, N., & Thiele, K. (2018). Innovative analysis of a buried operating pipeline subjected to strike-slip fault movement. Soil dynamics and earthquake engineering, 107, 234-249.

Bathurst, R. J., Allen, T. M., & Walters, D. L. (2002). Short-term strain and deformation behavior of geosynthetic walls at working stress conditions. Geosynthetics International, 9(5–6), 451–482.

Chatzidakis, D., Tsompanakis, Y., & Psarropoulos, P. N. (2022). Kinematic distress of pipelines subjected to secondary seismic fault rupture. Soil Dynamics and Earthquake Engineering, 152, 107065.

Cheuk, C. Y., White, D. J., & Bolton, M. D. (2008). Uplift mechanisms of pipes buried in sand. Journal of Geotechnical and Geoenvironmental Engineering, 134(2), 154–163.

Chin, E. L., Craig, W. H., & Cruikshank, M. (2006). Uplift resistance of pipeline buried in cohesionless soil. In Proceedings of the Sixth International Conference on Physical Modelling in Geotechnics (pp. xx–xx). London.

Chiou, Y., & Chi, S., Chang, H. (1994). A study on buried pipeline response to fault movement. Pressure Vessel Technology, ASME, 116, 36–41.

Demirci, H. E., Bhattacharya, S., Karamitros, D., & Alexander, N. (2018). Experimental and numerical modelling of buried pipelines crossing reverse faults. Soil Dynamics and Earthquake Engineering, 114, 198-214.

Dey, S., & Tesfamariam, S. (2022). Structural performance of buried pipeline undergoing fault rupture in sand using Taguchi design of experiments. Soil Dynamics and Earthquake Engineering, 155, 107174.

Farhang, M., & Jalali, H. H. (2025). Performance assessment of corroded buried pipelines under strike-slip faulting using stochastic wall loss modeling. *Soil Dynamics and Earthquake Engineering*, *199*, 109697.

Ha, D. (2007). Evaluation of ground rupture effect on buried HDPE pipelines (Doctoral dissertation, Rensselaer Polytechnic Institute). Rensselaer Polytechnic Institute Library.

Ha, D., Abdoun, T. H., O'Rourke, M. J., Symans, M. D., O'Rourke, T. D., Palmer, M. C., & Stewart, H. E. (2008). Buried high-density polyethylene pipelines subjected to normal and strike-slip faulting: A centrifuge investigation. Canadian Geotechnical Journal, 45, 1733–1742.

Ha, D., Abdoun, T. H., O'Rourke, M. J., Symans, M. D., O'Rourke, T. D., Palmer, M. C., & Stewart, H. E. (2010). Earthquake faulting effects on buried pipelines – case history and centrifuge study. Journal of Earthquake Engineering, 14, 646–669.

Hamada, M., & O'Rourke, T. (1992). Case studies of liquefaction and lifeline performance during past earthquakes. National Center for Earthquake Engineering Research, Technical Report NCEER-92-

0001, State University of New York at Buffalo.

Hayashi, M., Oda, K., & Miyajima, M. (2016). Characteristics of pipeline damages in the 2014 Northern Nagano Prefecture earthquake in Japan. In Proceedings of the 11th Pacific Conference on Earthquake Engineering (pp. 322–330). American Society of Civil Engineers. https://doi.org/10.1061/9780784480342.044

Itasca Consulting Group, Inc. (2012). *FLAC3D: Fast Lagrangian analysis of continua in 3 dimensions* (Version 5.0). Minneapolis, MN: Itasca Consulting Group.

Jahangiri, V., & Shakib, H. (2020). Reliability-based seismic evaluation of buried pipelines subjected to earthquake-induced transient ground motions. Bulletin of earthquake engineering, 18(8), 3603-3627.

Joshi, S., Prashant, A., Deb, A., & Jain, S. K. (2011). Analysis of buried pipelines subjected to reverse fault motion. *Soil Dynamics and Earthquake Engineering*, *31*(7), 930-940.

Karamitros, D. K., Bouckovalas, G. D., & Kouretzis, G. P. (2007). Stress analysis of buried steel pipelines at strike-slip fault crossings. Soil Dynamics and Earthquake Engineering, 27(3), 200–211.

Kennedy, R. P., Chow, A., & Williamson, R. A. (1977). Fault movement effects on buried oil pipeline. Journal of the Transportation Engineering Division, ASCE, 103(5), 617–633.

Kurtuluş, A. (2011). Pipeline vulnerability of Adapazarı during the 1999 Kocaeli, Turkey, earthquake. *Earthquake Spectra, 27*(1), 45–66. https://doi.org/10.1193/1.3541843

Lee, J. (2005). Study on earthquake fault rupture propagation through sandy soil deposit (PhD dissertation). Waseda University, Japan.

Liu, A. W., Hu, Y. X., Zhao, F. X., Li, X. J., Takada, S., & Zhao, L. (2004). An equivalent-boundary method for the shell analysis of buried pipelines under fault movement. Acta Seismologica Sinica, 17(1), 150–156.

Liu, X., Zhang, H., Li, M., Xia, M., Zheng, W., Wu, K., & Han, Y. (2016). Effects of steel properties on the local buckling response of high strength pipelines subjected to reverse faulting. Journal of Natural Gas Science and Engineering, 33, 378–387.

Melissianos, V. E., Korakitis, G. P., Gantes, C. J., & Bouckovalas, G. D. (2016). Numerical evaluation of the effectiveness of flexible joints in buried pipelines subjected to strike-slip fault rupture. Soil Dynamics and Earthquake Engineering, 90, 395–410.

Merry, S. M., & Bray, J. (2003). Time-dependent mechanical response of HDPE geomembranes. Journal of Geotechnical Engineering, ASCE, 123(1), 57–65.

Miyajima, M., Yoshifuji, Y., & Kitaura, M. (2003). Experiments on behaviors of buried pipeline subjected to surface fault rupture. In Proceedings of the Third Taiwan-Japan Workshop on Earthquake Resistant Design (pp. 53–60).

Murry, D. W. (1997). Strain localization, wrinkling and post buckling response of line pipe. Engineering Structures, 19(5), 360–371.

Naghdali, M., Bagherieh, A. R., & Bagherieh, A. (2020). Numerical modeling of wave feature to enhance the performance of buried steel pipelines subjected to faulting displacements. *Indian Geotechnical Journal, 50*(5), 739–752. https://doi.org/10.1007/s40098-020-00413-7

Newmark, N., & Hall, W. (1975). Pipeline design to resist large fault displacement. In Proceedings of U.S National Conference on Earthquake Engineering (pp. 416–425). University of Michigan.

Ng, C. W. W., & Springman, S. M. (1994). Centrifuge modeling of uplift resistance of buried pipelines in granular materials. In C. F. Leung, F. H. Lee, & T. S. Tan (Eds.), Centrifuge 94 (pp. 753–758). Balkema.

Nyman, K. J. (1983). Thaw settlement analysis for buried pipelines in permafrost. In Proceedings of the Conference on Pipelines in Adverse Environments — II (pp. 300–325). ASCE Pipeline Division.

O'Rourke, M. J., & Liu, X. (1999). Response of buried pipelines subject to earthquake effects. Monograph No. 3, Multidisciplinary Center for Earthquake Engineering Research, Buffalo, NY.

Qiu, C., Tian, S., & Wang, Y. (2025). Structural Failure and Mechanical Response of Buried Pipelines Under Offshore Fault Dislocation. Applied Sciences, 15(17), 9450.

Robert, D. J., & Rajeev, P. (2016). A modified Mohr-Coulomb model to simulate the response of buried pipes subjected to large ground displacement. In Geo-Chicago 2016 (pp. 410-421).

Saiyar, M., Ni, P., Take, W. A., & Moore, I. D. (2016). Response of pipelines of differing flexural stiffness to normal faulting. *Géotechnique*, *66*(4), 275-286.

Saiyar, M., Take, W. A., & Moore, I. D. (2011). Validation of boundary PIV measurements of soil–pipe interaction. International Journal of Physical Modelling in Geotechnics, 11(1), 23–32.

Savidis, S., Schepers, W., Nomikos, S., & Papadakos, G. (2011). Design of a natural gas pipeline subjected to permanent ground deformation at normal faults: A parametric study on numerical vs. semi-analytical procedures. 5th International Conference on Earthquake Geotechnical Engineering, Santiago, Chile.

Shakib, H., & Zia-Tohidi, R. (2004, August). Response of steel buried pipelines to three-dimensional fault movements by considering material and geometrical nonlinearities. In Proceedings of the 13th World Conference on Earthquake Engineering, Vancouver, BC, Canada (pp. 1–6).

Tahghighi, H., & Hajnorouzi, M. (2014). Numerical evaluation of the strike-slip fault effects on the steel buried pipelines. Journal of Seismology and Earthquake Engineering, 16(4), 219.

Takada, S., Hassani, N., & Fukuda, K. (2001). A new proposal for simplified design of buried steel pipes crossing active faults. Earthquake Engineering & Structural Dynamics, 30(8), 1243–1257.

Takada, S., Liang, J. W., & Li, T. (1998). Shell-mode response of buried pipelines to large fault movements. Journal of Structural Engineering, 44(1), 1.

Talebi, F., & Kiyono, J. (2021). Comparison of 3D Solid and Beam–Spring FE Modeling Approaches in the Evaluation of Buried Pipeline Behavior at a Strike-Slip Fault Crossing. *Energies*, *14*(15), 4539.

Tang, A. (Ed.). (2000). *Izmit (Kocaeli), Turkey, earthquake of August 17, 1999, including Düzce earthquake of November 12, 1999—Lifeline performance* (Monograph No. 17). American Society of Civil Engineers.

Trifonov, O. V., & Cherniy, V. P. (2010). A semi-analytical approach to a nonlinear stress–strain analysis of buried steel pipelines crossing active faults. Soil Dynamics and Earthquake Engineering, 30(11), 1298–1308.

Trifonov, O. V., & Cherniy, V. P. (2012). Elastoplastic stress–strain analysis of buried steel pipelines subjected to fault displacements with account for service loads. Soil Dynamics and Earthquake Engineering, 33(1), 54–62.

Uckan, E., Akbas, B., Shen, J., Rou, W., Paolacci, F., & O'rourke, M. (2015). A simplified analysis model for determining the seismic response of buried steel pipes at strike-slip fault crossings. Soil Dynamics and Earthquake Engineering, 75, 55-65.

Vazouras, P., Dakoulas, P., & Karamanos, S. A. (2015). Pipe–soil interaction and pipeline performance under strike–slip fault movements. Soil Dynamics and Earthquake Engineering, 72, 48–65.

Vazouras, P., Karamanos, S. A., & Dakoulas, P. (2012). Mechanical behavior of buried steel pipes crossing active strike-slip faults. Soil Dynamics and Earthquake Engineering, 41, 164–180.

Vazouras, P., Karamanos, S., & Dakoulas, P. (2010). Finite element analysis of buried steel pipelines under strike-slip fault displacements. Soil Dynamics and Earthquake Engineering, 30, 1361–1376.

Wang, L., & Yeh, Y. (1985). A refined seismic analysis and design of buried pipeline for fault movement. Earthquake Engineering and Structural Dynamics, 13, 75–96.

Warren, K. A., Christopher, B., & Howard, I. L. (2010). Geosynthetic strain gage installation procedures and alternative strain measurement methods for roadway applications. Geosynthetics International, 17(6), 403–430.

Wham, B. P., O'Rourke, T. D., Stewart, H. E., Bond, T. K., Pariya-Ekkasut, C., & Hall, H. (2016). Large-scale testing of JFE steel pipe crossing faults: Testing of SPF wave feature to resist fault rupture.

White, D. J., Barefoot, A. J., & Bolton, M. D. (1994). Centrifuge modelling of upheaval buckling in sand. International Journal of Physical Modelling in Geotechnics, 2, 19–28.

Wijewickreme, D., & Dilrukshi, S. (2017). Effect of pipe size on estimating soil restraint on pipelines subject to transverse permanent ground movements. In Proceedings of the 19th International Conference on Soil Mechanics and Geotechnical Engineering (ICSMGE 2017).

Winkler, E. (1867). *Die Lehre von der Elasticität und Festigkeit* [The theory of elasticity and strength]. Prague: H. Dominicus.

Xie, X. (2008). Numerical analysis and evaluation of buried pipeline response to earthquake-induced ground fault rupture (Doctoral dissertation, Rensselaer Polytechnic Institute).

Xie, X., Symans, M. D., O'Rourke, M. J., Abdoun, T. H., O'Rourke, T. D., Palmer, M. C., & Stewart, H. E. (2011). Numerical modeling of buried HDPE pipelines subjected to strike-slip faulting. *Journal of Earthquake Engineering, 15*(8), 1273–1296.

Xie, X., Symans, M. D., O'Rourke, M. J., Abdoun, T. H., O'Rourke, T. D., Palmer, M. C., & Stewart, H. E. (2011). Numerical modeling of buried HDPE pipelines subjected to strike-slip faulting. Journal of Earthquake Engineering, 15(8), 1273-1296.

Yimsiri, S., Soga, K., Yoshiaki, K., Dasari, G. R., & O'Rourke, T. D. (2003). Lateral and upward soil-pipeline interactions in sand for deep embedment conditions. Journal of Geotechnical and Geoenvironmental Engineering, 130, 830–841.

Zhang, D. F., Bie, X. M., Zeng, X., Lei, Z., & Du, G. F. (2020). Experimental and numerical studies on mechanical behavior of buried pipelines crossing faults. Structural Engineering and Mechanics, An Int'l Journal, 75(1), 71-86.